Anderson localization of light in disordered superlattices containing graphene layers

A. J. Chaves* and N. M. R. Peres†
Department of Physics and Center of Physics, University of Minho, P-4710-057 Braga, Portugal

F. A. Pinheiro‡
Instituto de Física, Universidade Federal do Rio de Janeiro, Rio de Janeiro-RJ 21941-972, Brazil
and Optoelectronics Research Centre and Centre for Photonic Metamaterials, University of Southampton, Highfield, Southampton SO17 1BJ, United Kingdom

(Received 24 September 2015; published 23 November 2015)

We perform a theoretical investigation of light propagation and Anderson localization in one-dimensional disordered superlattices composed of dielectric stacks with graphene sheets in between. Disorder is introduced either on graphene material parameters (e.g., Fermi energy) or on the widths of the dielectric stacks. We derive an analytic expression for the localization length ξ, and we compare it to numerical simulations using the transfer-matrix technique; a very good agreement is found. We demonstrate that the presence of graphene may strongly attenuate the anomalously delocalized Brewster modes, and it is at the origin of a periodic dependence of ξ on frequency, in contrast to the usual asymptotic decay, $\xi \propto \omega^{-2}$. By unveiling the effects of graphene on Anderson localization of light, we pave the way for new applications of graphene-based, disordered photonic devices in the THz spectral range.

DOI: 10.1103/PhysRevB.92.195425 PACS number(s): 42.25.Dd, 78.20.−e, 73.20.Fz

I. INTRODUCTION

Due to its extraordinary electronic and optical properties, graphene has emerged as an alternative material platform for applications in photonics and optoelectronics [1–3]. A partial but by no means exhaustive list of applications of graphene in photonics includes high-speed photodetectors [4], optical modulators [5], plasmonic devices [6–8], and ultrafast lasers [9]. In addition, graphene is a promising candidate to overcome one of the major existing hurdles to bring optics and electronics together, namely the efficient conversion between optical and electronic signals. Indeed, this can be facilitated by the fact that graphene enables strong, electric field-tunable optical transitions, and it resonantly enhances light-matter interactions in subwavelength volumes. In practice, this can be achieved, for instance, by integrating a graphene layer into a photonic crystal nanocavity [10]. The presence of graphene also allows for an efficient electro-optical modulation of photonic crystal nanocavities by electrostatic gating [11,12]. However, the integration of graphene into photonic crystals is naturally prone to unavoidable disorder associated with the fabrication process. This constitutes *per se* a motivation to investigate the effects of disorder in photonic crystals containing graphene layers, which, as far as we know, have not been considered in the literature so far. In addition to this technological and practical motivation, there is a very fundamental one as well, namely to understand the impact of graphene on Anderson localization of light.

The concept of Anderson localization (AL) was originally conceived in the realm of condensed-matter physics as a disorder-driven metal-insulator transition [13]. Being an interference wave phenomenon, this concept has been extended to light [14–16], acoustic waves [17], and even Bose-Einstein condensed-matter waves [18]. As a result, Anderson localization is today a truly interdisciplinary topic, and important contributions have emerged from different areas, ranging from condensed matter, photonics, acoustics, atomic physics, and seismology [19]. Dimensionality is crucial to AL, and in one dimension the vast majority of states is exponentially localized on a length scale given by the localization length ξ, regardless of the disorder strength. In optical systems exceptions do exist, and delocalized modes may occur in low-dimensional systems as a result of the presence of correlations [20], necklace modes [21], or metamaterials with negative refraction [22–26]. The question of whether these anomalies occur when graphene is integrated into disordered optical superlattices remains unresolved.

Bearing in mind both these technological and fundamental motivations, in the present paper we undertake an analytical and numerical investigation of Anderson localization of light in one-dimensional disordered superlattices composed of dielectric stacks with graphene layers in between, as depicted in Fig. 1. We consider two possible, realistic ways to model disorder: compositional and structural disorder. In the former case, disorder is introduced in graphene's material parameters, such as the Fermi energy, whereas in the latter the dielectric components of the superlattice have random widths. In both cases, we derive an analytic expression for the localization length ξ, and we compare it to numerical simulations using a transfer-matrix technique; an overall very good agreement is found. In the case in which the medium impedances match, we find that ξ exhibits oscillatory behavior as a function of frequency ω, in contrast to the usual asymptotic decay $\xi \propto \omega^{-2}$. In the study of electromagnetic localization in dispersive stratified media, and for large wavelength when compared to the unit-cell length, similar oscillatory behavior has been found [27]. We demonstrate that graphene may strongly suppress the anomalously delocalized Brewster modes, as it induces additional reflections at the superlattice interfaces. We also

*andrej6@gmail.com
†peres@fisica.uminho.pt
‡fpinheiro@if.ufrj.br

 ©2015 American Physical Society

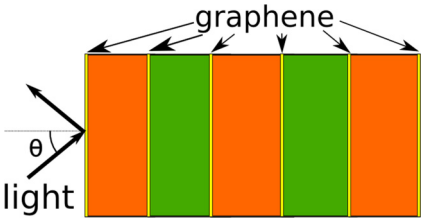

FIG. 1. (Color online) Schematic representation of the system.

investigate the effects of interband and intraband transitions of the graphene conductivity on ξ, identifying the regimes where Anderson localization and absorption dominates light transmission. In the first case, the real part of the graphene conductivity is negligible, whereas in other cases it is not.

This paper is organized as follows. In Sec. II we present the analytical results, where we derive an expression for the localization length of disordered superlattices containing graphene sheets. In Sec. III we present and discuss the numerical simulations, based on the transfer-matrix technique, which are also compared to the analytical calculations. Finally, Sec. IV is devoted to the concluding remarks. We also present a number of Appendixes giving the details of the calculations and aiming at making the text as self-contained as possible. To the best of our knowledge, there are only two published papers [28,29] dealing with similar problems to the one we consider in this paper, but in the context of metals, in which case only Drude's conductivity plays a role.

II. ANALYTICAL CALCULATION OF THE LOCALIZATION LENGTH

Light propagation in a one-dimensional (1D) superlattice containing graphene layers (Fig. 1) is modeled by the transfer-matrix formalism [30]. The $M^n = \{m^n_{ij}\}$ transfer matrix connects the fields at the right of the nth unit cell to those at left according to

$$\psi^{n+1} = M^n \psi^n, \tag{1}$$

where $\psi^n = [\psi^n_R \quad \psi^n_L]^T$, and ψ^n_R (ψ^n_L) refers to the right (left) propagating field in the nth cell. For transverse electric (TE) and transverse magnetic (TM) modes, ψ refers to the electric and magnetic field, respectively. We consider the particular case in which $\det M^n = 1$, which occurs for systems with preserved time-reversal symmetry [30]. In this case, one can show that M^n may be written as

$$M^n = \begin{pmatrix} \cosh\phi^n_1 e^{i\phi^n_2} & \sinh\phi^n_1 e^{i\phi^n_3} \\ \sinh\phi^n_1 e^{-i\phi^n_3} & \cosh\phi^n_1 e^{-i\phi^n_2} \end{pmatrix}, \tag{2}$$

where ϕ^n_i are parameters that depend on the composition of the nth cell. (From here on we omit the n dependence in ϕ_i, except when strictly necessary to avoid any confusion.) For periodic systems with preserved time-reversed symmetry, ϕ_i are real numbers and all the M^n's are equal. We thus write $M^n = M^0$. One can write the photonic dispersion relation [30] as $\cos\gamma = (m^0_{11} + m^0_{22})/2$, where

$$\cos\gamma = \cosh\phi^0_1 \cos\phi^0_2. \tag{3}$$

Disorder is introduced in the parameters ϕ_i:

$$\phi_i = \phi^0_i + \delta\phi_i, \tag{4}$$

where $\delta\phi_i$ describes random fluctuations around the average value, and which may have different origins, as will be detailed later in the paper. For a periodic system, a transformation $M_{\text{transf}} = M_{\text{circle}} M_{\text{real}}$ (see Appendix A) exists that maps the variables $\psi^n_{R,L}$ into a new set of variables, denoted by Q_n and P_n, such that $X^T = [Q^n \; P^n]^T = M_{\text{transf}}[\psi^n_R \; \psi^n_L]^T$. These new variables describe a circle in phase space [31], with radius $\sqrt{Q^2_n + P^2_n}$ proportional to the electric field amplitude. Applying this transformation to Eq. (1), the transformed matrix $M' = M_{\text{transf}} M^n M^{-1}_{\text{transf}}$ reads

$$M' = \begin{pmatrix} E_n & F_n \\ G_n & H_n \end{pmatrix}, \tag{5}$$

where

$$E_n = \cosh\phi_1 \cos\phi_2 - \sinh\phi_1 \sin\delta\phi_3, \tag{6}$$

$$F_n = -v^2(\cosh\phi_1 \sin\phi_2 + \sinh\phi_1 \cos\delta\phi_3), \tag{7}$$

$$G_n = v^{-2}(\cosh\phi_1 \sin\phi_2 - \sinh\phi_1 \cos\delta\phi_3), \tag{8}$$

$$H_n = \cosh\phi_1 \cos\phi_2 + \sinh\phi_1 \sin\delta\phi_3 \tag{9}$$

with v and τ defined in Appendix A. When $\phi_i = \phi^0_i$, we have $\delta\phi_3 = 0$, and Eqs. (6)–(9) lead to $E_n = H_n = \cos\gamma$ and $F_n = -G_n = \sin\gamma$. When weak disorder is introduced, the trajectory of the points (Q_n, P_n) results in a perturbation of the circle. The recurrence equations defined by $X^{n+1} = M' X^n$ are similar to a Hamiltonian map of the classical harmonic oscillator subjected to a parametric impulsive force [32], where Q_n and P_n are the coordinate and conjugated moments, respectively, and γ is the phase between successive kicks.

The presence of disorder introduces a key length scale, the localization length ξ. In 1D electronic systems, all eigenmodes are exponentially localized, although some exceptions do exist in the realm of optical systems [21,22,24,25] (see the Introduction). The length ξ characterizes the exponential decay of the eigenfunctions and is defined in terms of the reciprocal of the Lyapunov exponent λ. In one dimension, λ can be written as [30,31]

$$\lambda = \frac{1}{2}\left\langle \ln\left|\frac{\psi^{n+1}_R}{\psi^n_R}\right|^2 \right\rangle. \tag{10}$$

In Eq. (10), the angular brackets denote averaging over both ensembles and the system unit cells, while the usual definition of the localization length considers only averages over ensembles [30]. The two definitions are equivalent. The relation between λ and ξ is

$$\lambda = \frac{d}{\xi}, \tag{11}$$

where d is the mean length of the unit cell. The advantage of the approach based on the parameters P_n and Q_n is that we can use polar (or action-angles) coordinates:

$$P_n = R_n \sin\Theta_n, \quad Q_n = R_n \cos\Theta_n. \tag{12}$$

Without disorder, R_n is a constant and Θ_n increases by minus the Bloch phase, $-\gamma$, as we move from unit cell to

unit cell. With disorder, the radius R_n changes in every step, with R_{n+1} a function of R_n, Θ_n, and of the matrix elements of M^n. The angle Θ_{n+1} only depends on Θ_n and M^n. For weak disorder, a recurrence equation (B9) exists that, in the continuum limit, becomes a stochastic Îto equation that has a corresponding Fokker-Planck equation [33]. In this case, the first approximation for the density probability function of Θ_n is uniform in the interval $[0,2\pi]$ for $\gamma \neq 0,\pi/2,\pi$.

Writing Eq. (10) in terms of R and Θ, and averaging over Θ with uniform density probability, we obtain, up to second order in $\delta\phi_i$,

$$\lambda = \tfrac{1}{2}\big\langle Y_1 + Y_2\cos 2\Theta_n + Y_3 \sin 2\Theta_n - \tfrac{1}{4}Y_2^2 - \tfrac{1}{4}Y_3^2\big\rangle, \quad (13)$$

where Y_i, with $i = 1,2,3$ defined in Appendix B and depending on the matrix elements M^n.

In the following sections, we will study the propagation of light through a disordered structure of alternating graphene sheets and dielectric layers. In this case, each propagation matrix M^n is determined by the widths z_i, the incidence angle θ_i, the dielectric material parameters μ_i and ε_i, and the graphene conductivity σ. In the present work, we focus on the cases in which disorder is present in the widths of the stacks (structural disorder) and on graphene conductivities (compositional disorder). Both are realistic situations that may occur in the fabrication of these structures.

For the type of structural disorder studied here, the width of each layer i of the nth cell is a random variable,

$$z_i(n) = z_i^0 + \zeta_i(n), \quad (14)$$

where ζ_i are uncorrelated random variables with zero mean and mean standard deviation σ_i: $\langle[\zeta_i(n)]^2\rangle = \sigma_i^2$; z_i^0 is the mean width of the i slab (the standard deviation σ_i should not be confused with graphene's conductivity σ).

In the case of compositional disorder, the Fermi energy E_F is a random variable in each layer n,

$$E_F(n)/\hbar = \omega_F(n) = \omega_F^0 + \zeta_F(n), \quad (15)$$

with ζ_F a random variable with zero mean and $\langle\zeta_F^2\rangle = \sigma_F^2$. This determines how the graphene conductivity, given in Appendix D, is affected by disorder.

In the next section, we derive analytical expressions for λ [Eq. (13)] in different regimes. Toward that end, we need to map ϕ_i in the system variables, calculate the differentials δ_i, and use the results given in Appendix B.

A. Unit cell made of two different dielectric materials and a graphene sheet at the interface

We consider a disordered superlattice composed of dielectric bilayers with a graphene sheet in between. The transfer matrix for the n unit cell is given by $M^n = \{m_{jl}^n\}$ and is explicitly derived in Appendix C 1.

To proceed with the calculation of the Lyapunov exponent, it is necessary to map the system parameters of the transfer matrix (C1) into the parametric matrix (2). There is not a unique way of doing this, but in what follows we make the simplest choice.

1. Disordered photonic superlattice without graphene

To model a disordered photonic superlattice without the graphene layer, we set $f = 0$ in Eq. (C1) and map ϕ_i into the system parameters $\alpha_1,\alpha_2,\chi,\Delta$ (defined in Appendix C):

$$\begin{aligned}\sinh\phi_1 &= \Delta^x \sin\alpha_2,\\ \phi_2 &= \alpha_1 + \arctan(\chi^x \tan\alpha_2),\\ \phi_3 &= \alpha_1 + \pi/2,\end{aligned} \quad (16)$$

where x = TE,TM. According to this mapping, we can replace ϕ_i in the expressions for Y_i in Appendix B and calculate the differentials $\delta\phi_i$ using Eq. (14) with $\zeta_i \ll z_i^0$. This will enable us to compute the Lyapunov exponent, given by Eq. (13); the final result is

$$\lambda = \frac{\Delta^2}{2\sin^2\gamma}\big(\sin^2\alpha_2\, k_1^2\,\sigma_1^2 + \sin^2\alpha_1\, k_2^2\,\sigma_2^2\big), \quad (17)$$

which agrees with the result of Ref. [31] for uncorrelated disorder. The described procedure is repeated to calculate the Lyapunov exponents in the next sections.

2. Disordered superlattice containing graphene layers

The presence of graphene at the interface between the dielectrics results in a discontinuity in the tangential component of the magnetic field. This condition can be obtained from the Maxwell equation $\nabla \times \mathbf{H} = \sigma\delta(z)\mathbf{E} - i\omega\mathbf{D}$. The Dirac δ function in the previous equation introduces a divergence in the derivative of the field that corresponds to a discontinuity in the tangential components of the magnetic field. This discontinuity is proportional to the surface current density in the graphene sheet, which depends on the optical conductivity of the material.

The role of graphene on the optical properties of the superlattice increases as the value of the dimensionless parameter $\beta_i^x f$ increases, with $f = \sigma c\mu_0/2$ and β_i^x given in Appendix C. We are interested in the lossless regime in which the Bloch phase γ, given by Eq. (C3), is real. This regime sets up when (i) σ (and therefore f) is a pure complex number and θ_i, with $i = 1,2$, is a pure real number; or (ii) σ is a pure real number so that evanescent propagation occurs in one of the layers.

In the first case, we define $B^x = i\tilde{B}^x$ (see Appendix C), where $\tilde{B}$ is real, and we map the parameters ϕ_i in

$$\begin{aligned}\sinh\phi_1 &= -\tilde{B}^x\cos\alpha_2 + (\Delta - D^x)\sin\alpha_2,\\ \phi_2 &= \alpha_1 + \arg[A_+^x\cos\alpha_2 + i(\chi + C_+^x)\sin\alpha_2],\\ \phi_3 &= \alpha_1 + \pi/2.\end{aligned} \quad (18)$$

Following the procedure of Sec. II A 1, the Lyapunov exponent is given by

$$\lambda = \frac{1}{2\sin^2\gamma}\big(K_2^2 k_1^2\sigma_1^2 + K_1^2 k_2^2\sigma_2^2\big), \quad (19)$$

where

$$K_1 = -2\tilde{f}\lambda^x\beta_2^x\cos\alpha_1 + \big[-\Delta + 2\tilde{f}^2\lambda^x\beta_1^x\beta_2^x\big]\sin\alpha_1, \quad (20)$$

and $f = i\tilde{f}$; K_2 is obtained by interchanging $1 \leftrightarrow 2$ and $\Delta \to -\Delta$. Notice that if one plugs Eq. (20) with $f = 0$ into Eq. (19), Eq. (17) is obtained, as it should be.

B. Unit cell made of one dielectric material and a graphene sheet at the interface

For systems composed of bilayers of the same dielectric material with a graphene sheet in between, it is much easier to calculate the transfer matrix, which is given in Eq. (C9). In this case, the ϕ_i parameters read

$$\begin{aligned} \sinh\phi_1 &= -\lambda^x \beta^x \tilde{f}, \\ \phi_2 &= \alpha, \\ \phi_3 &= \alpha + \pi/2. \end{aligned} \tag{21}$$

Using Eq. (13) and the results of Appendix B, we calculate the Lyapunov exponent for structures containing both random graphene conductivities (compositional disorder) and random widths (structural disorder), as detailed in the following.

1. Compositional disorder

Using the same procedure of Sec. II A 1, we obtain the Lyapunov exponent:

$$\lambda = \frac{1}{2}\left(\frac{\sin 2\alpha}{\sin 2\gamma}\beta^x \frac{\pi\alpha_c}{2}\sigma_g\right)^2, \tag{22}$$

where α_c is the fine-structure constant and σ_g is the mean standard deviation of the normalized graphene conductivity,

$$\sigma_g^2 = \frac{\langle\sigma^2\rangle - \langle\sigma\rangle^2}{\sigma_0^2}. \tag{23}$$

2. Structural disorder

For structural disorder where the stacks' widths are given by Eq. (14), the Lyapunov exponent reads

$$\lambda = \frac{\tilde{f}^2\beta^{x\,2}k^2\sigma^2}{2\sin^2\gamma}. \tag{24}$$

This concludes the analytical part of our work, which will be compared to numerical simulations in the following section.

III. NUMERICAL SIMULATIONS: RESULTS AND DISCUSSIONS

A. Simulation procedure

The numerical calculations are based on the transfer-matrix method; the total transfer matrix for light propagating in an N-layered system is

$$M = \Pi_{n=1}^{N} M^n, \tag{25}$$

where the elements of M^n are given by Eq. (C1). Transmission is calculated by applying the boundary condition related to the fact that there is no incoming wave from the left:

$$T = \frac{1}{|m_{22}|^2}, \tag{26}$$

and the localization length ξ is calculated by

$$\frac{L}{\xi} = -\frac{1}{2}\langle\ln T\rangle, \tag{27}$$

where $L = Nd$ and N is the total number of unit cells with mean width d. The length L is chosen to be large enough to ensure that the numerical calculation of the localization length converges. In the numerical procedure, we first generate random variables ζ_i (or ζ_F) [see Eqs. (14) and (15)] from a uniform distribution, and then we calculate the transfer matrix using Eq. (25). With the help of the results introduced in Appendix C, we obtain the localization length using Eq. (27). The procedure is repeated over n_{samples}, and the mean value of the localization length is calculated. We have verified that, for a sufficiently large N, the value of ξ calculated for a single disorder realization coincides with its average over many disorder realizations for smaller systems; in other words, we have verified that ξ is a self-averaging quantity. Also, we have verified the convergence of the localization length with the number N of cells. Further details of the transfer-matrix method are given in Appendix C.

B. Results

Light transmission depends on the graphene conductivity σ and on the medium impedances, defined as (see Appendix C)

$$Z_i^{\text{TE}} = \frac{\sqrt{\mu_i\varepsilon_i}}{\mu_i}\cos\theta_i, \quad Z_i^{\text{TM}} = \frac{\sqrt{\mu_i\varepsilon_i}}{\varepsilon_i}\cos\theta_i. \tag{28}$$

We will focus in the lossless regime with $\text{Im}\cos\gamma = 0$ and $\text{Re}\cos\gamma \leqslant 1$. From Eq. (C3), this regime occurs whenever f (and consequently σ) is a pure complex number or for $\text{Im}\sigma = 0$, in which case one of the slabs supports an evanescent mode. When the Drude term dominates, the imaginary part of the conductivity is positive (see Appendix D). For frequencies slightly below $2\omega_F$, the interband term dominates and the imaginary part of the conductivity is negative (see Appendix D). When the frequency becomes larger than $2\omega_F$, the imaginary part goes to zero and the real part tends to $\sigma_0 = e^2/4h$.

In the following numerical calculations, random variables have a uniform distribution with $\zeta_x \in [-\Upsilon_x/2, \Upsilon_x/2]$, with $x = 1,2$ for structural disorder and $x = F$ for compositional disorder.

C. Drude regime when $\text{Re}\,\sigma \approx 0$, $\text{Im}\,\sigma > 0$

When $\omega_F\Gamma \ll \omega^2 \ll \omega_F^2$ (where Γ is the broadening entering in the conductivity), graphene conductivity can be approximated by (see Appendix D 1)

$$\sigma = i\sigma_0\frac{4}{\pi}\frac{\omega_F}{\omega}. \tag{29}$$

For $E_F \approx 0.3$ eV (a typical value for the graphene Fermi energy), the range of frequencies corresponds to the infrared spectral regime. In the following, we focus in three regimes: impedance matching in the double-layered system [$Z_1 = Z_2$, in Eq. (28)] with structural disorder, compositional disorder in the one-layered system, and the attenuated field regime (ATR) with structural disorder.

1. Impedance matching in the two-layered system with structural disorder

Using the Snell-Descartes law, Eq. (C2), and the impedances in Appendix C, one can verify that for materials without magnetic response ($\mu_1 = \mu_2 = 1$), there is no TE mode that allows the impedance matching. In the TM mode,

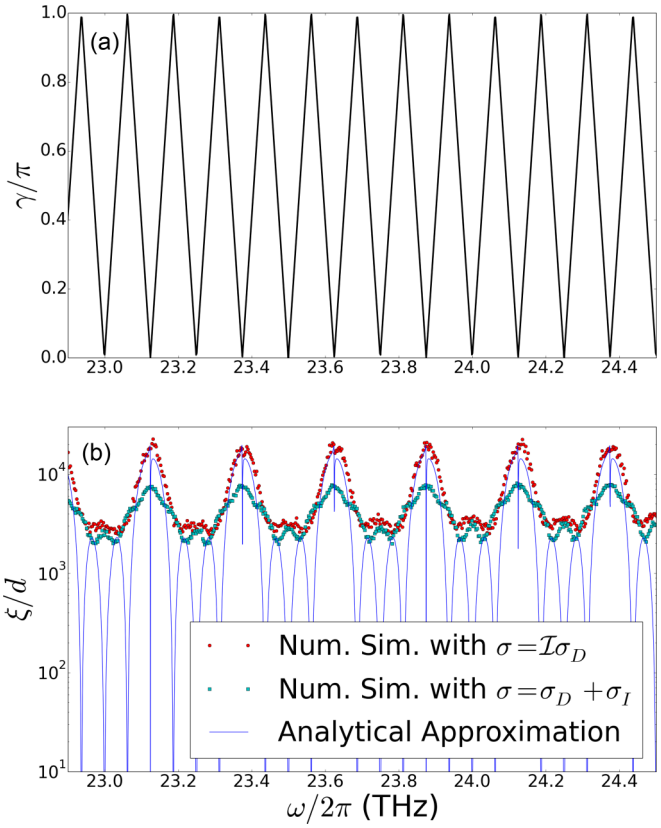

FIG. 2. (Color online) (a) Dispersion relation in the impedance matching regime and TM mode. (b) Localization length as a function of frequency with $\Upsilon_i = 5\ \mu$m, $z_i^0 = 1.2$ mm, $E_F = 0.2$ eV, $\Gamma = 260.0\ \mu$eV, $N = 5000$, $n_{\text{samples}} = 100$, $\varepsilon_1 = \mu_1 = \mu_2 = 1$, $\varepsilon_2 = 3$, and $\theta = \pi/3$.The solid line in (b) is the analytical result, whereas the dots correspond to two different numerical simulations for different regimes of the optical conductivity of graphene: (i) $\sigma = \text{Im}m\sigma_D$ (red points) and (ii) $\sigma = \sigma_D + \sigma_I$ (blue points).

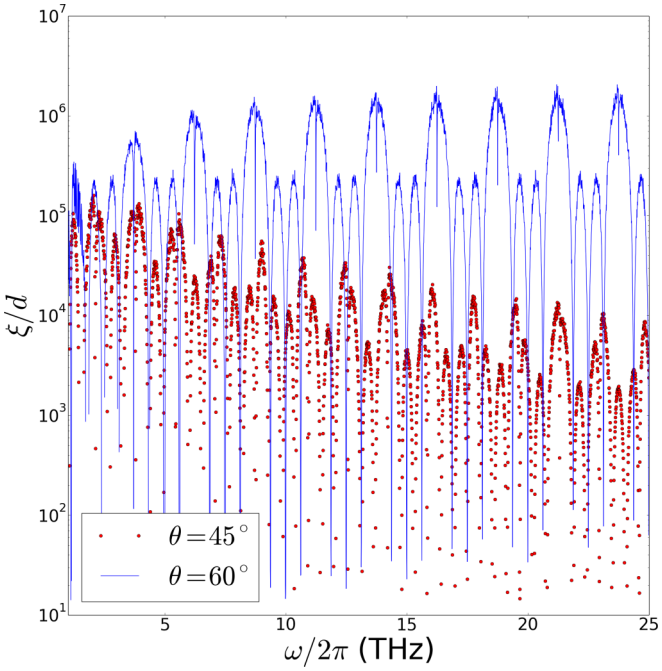

FIG. 3. (Color online) Localization length as a function of frequency in the impedance matched regime for two values of the incidence angle: $\theta = 60^\circ$ (blue line) and $\theta = 45^\circ$ (red circles). $\Upsilon_i = 0.5\,\mu$m, $z_i^0 = 120\,\mu$m, $E_F = 0.2$ eV, $\Gamma = 0.0\,\mu$eV, $N = 5000$, and $n_{\text{samples}} = 100$.

the impedance matching occurs when the angle of incidence in layer 1 obeys the relation $\sin^2\theta_1 = \varepsilon_2/(\varepsilon_1 + \varepsilon_2)$ for $\varepsilon_1 \neq \varepsilon_2$.

When $Z_i = Z$, $\beta_i = \beta$, it follows from Eqs. (19) and (20) that

$$\lambda = 2\left(\frac{4\tilde{f}\beta^x\omega_F}{\pi c \sin\gamma}\right)^2 \sum_{i=1}^{2} \varepsilon_i\mu_i \cos^2\alpha_i \cos^2\theta_i\sigma_i^2, \qquad (30)$$

where we neglected the term $\tilde{f}^2$ in comparison to $\tilde{f}$ (which in the Drude regime is always valid for sufficiently large ω). In this case, in Fig. 2(b) the localization length ξ is calculated, both analytically and numerically, as a function of frequency. The dispersion relation is also shown in Fig. 2(a). It is important to point out that the agreement between the analytical and numerical calculations is very good, except when γ approaches 0 or π. This is due to the fact that, in the analytical derivation of the Lyapunov exponent, the recurrence equation (B9) is ill-defined at these points, so that the distribution of random variables is not uniform. Remarkably, Fig. 2(b) reveals that in the impedance matching regime, ξ does not follow the well-known asymptotic power-law ω^{-2} behavior for low frequencies. Rather, ξ exhibits a periodic dependence on ω for low frequencies, a result that is intrinsically related to the graphene conductivity properties. Indeed, it can be explained by the fact that the linear increase of the wave number with frequency is canceled by the simultaneous decrease of graphene's conductivity [Drude term, see Eq. (29)], which scales with $1/\omega$. The periodicity in ξ follows from the periodicity in the dispersion relation, shown in Fig. 2(a). For the lossy and Drude regimes, ξ approaches the same value as the frequency increases, and the real part of the Drude conductivity goes to zero.

Figure 3 shows ξ as a function of frequency for two different values of the incidence angle θ. It reveals that the presence of graphene layers also has an important effect in the so-called Brewster modes in disordered systems. In 1D disordered optical systems, the so-called Brewster modes occur at some specific frequencies and incident angles for which ξ reaches anomalously high values, larger than the system size [24,34]. For nonmagnetic ($\mu_1 = \mu_2 = 1$) superlattices made of positive refractive-index media, these anomalously delocalized modes arise from the suppression of reflection at the interfaces of a 1D disordered system illuminated by a TM incident wave [24,34]. As a result, the system becomes fully transparent. The presence of graphene induces additional reflections at each interface of the superlattice, resulting in an attenuation of this Brewster mode, as can be seen from Fig. 4.

2. *ATR regime in the one-layered system*

The plasmon-polariton mode in graphene can be excited, for example, by a prism in the Otto configuration [35]. This is the regime we will explore in this section. We consider a periodic array of graphene/air unit cells (medium 2) in between

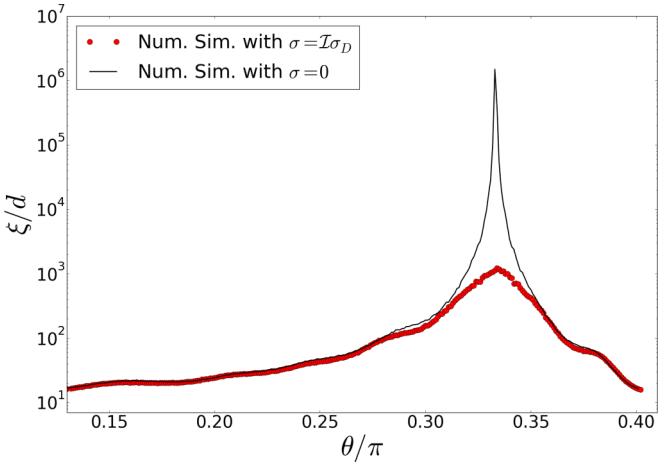

FIG. 4. (Color online) Localization length as a function of incidence angle in the impedance matched regime in the vicinities of a Brewster mode. $\Upsilon_i = 50\ \mu$m, $z_i^0 = 120\ \mu$m, $N = 5000$, and $n_{\text{samples}} = 100$. The black solid line corresponds to the grapheneless case; red circles correspond to the case in which graphene is present in the superlattice ($E_F = 0.2$ eV and $\Gamma = 0$ eV).

a dielectric (medium 1). In this case, the total transfer matrix M is obtained considering the boundaries between the prism and the superlattice:

$$M = M_{1\to 2} \prod_j (M_j)\, M_{2\to 1}, \tag{31}$$

where $M_{1\to 2}$ refers to the transfer matrix describing light propagation from the medium 1 (dielectric) to medium 2 (air); $M_{2\to 1}$ refers to the reverse propagation. M_j is the transfer matrix of the unit cell air/graphene with random widths (medium 2).

From Eq. (C10), one can see that for the evanescent mode α is a pure complex number and the first term on the right-hand side becomes a hyperbolic cosine, which is greater than 1 for any α. As a result, the Bloch phase is real only if the second term on the right-hand side of (C10) is negative. This situation occurs for pure positive complex f; in this case, β is also a pure positive complex number, which is only possible in the TM mode [see Eqs. (32) and (C4)].

For an incidence angle θ_1 above the critical angle for total reflection at the interface 1/2, a plasmon-polariton can be excited, allowing for frustrated total internal reflection. In this case, light propagation occurs due to the presence of periodic graphene sheets. The effective impedance in medium 2 depends on the properties of layer 1 as

$$Z_2^{\text{TE}} = i\frac{\kappa}{\mu_2}, \quad Z_2^{\text{TM}} = i\frac{\kappa}{\varepsilon_2}, \tag{32}$$

where

$$\kappa = \sqrt{\varepsilon_1\mu_1 \sin^2\theta_1 - \varepsilon_2\mu_2}. \tag{33}$$

In Fig. 5, the localization length is calculated in the ATR regime using both numerical and analytical methods; the agreement is excellent. In the Drude regime, ξ is inversely proportional to the Fermi energy. Also shown is the localization length when the dielectric necessary to excite the ATR field is removed; we call this situation the normal field. The ATR field is

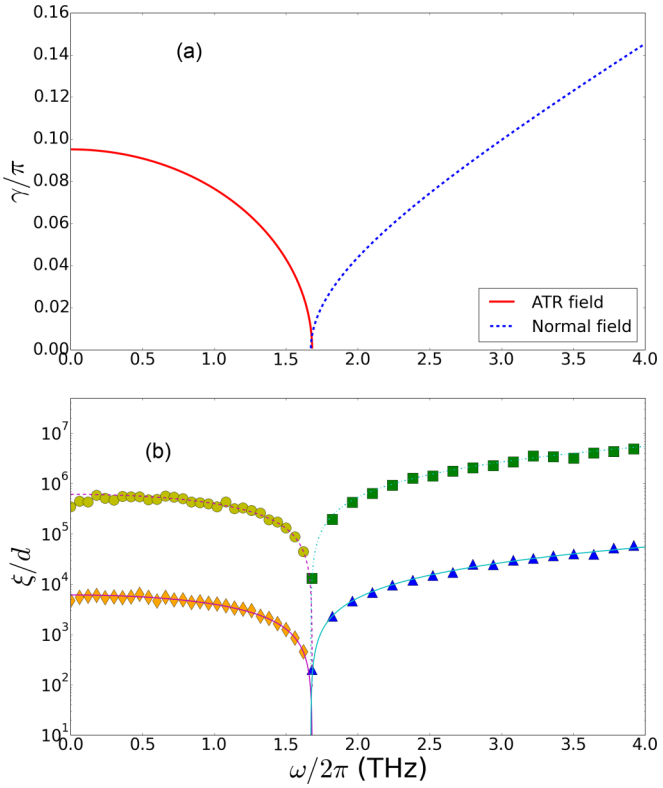

FIG. 5. (Color online) (a) Dispersion relation for the ATR regime (red) and for the normal field (blue). (b) Localization length as a function of frequency for $z^0 = 12\ \mu$m, $E_F = 0.1$ eV, $\theta_1 = \pi/3$, $\varepsilon_1 = 2$, $\mu_1 = \mu_2 = \varepsilon_1 = 1$, $N = 50\,000$, and $n_{\text{samples}} = 1$. The yellow circles (green squares) and orange diamonds (blue triangles) refer to the ATR (normal) field with $\Upsilon = 0.5$ and 5 μm, respectively. The cyan and purple lines refer to the analytical approximation.

characterized by exponentials with argument $\pm\omega\kappa z/c$. When the frequency increases and the length $c/\kappa\omega$ becomes smaller than the width z of the dielectric slab (air in this case), light propagation comes to a halt, as the plasmon-polariton localized in a graphene layer cannot excite the adjacent layer. We can see that the ATR for the parameters of Fig. 5 fills the band gap of the normal field. Also, the increase of disorder implies the decrease of ξ, as expected.

Notice that ignoring the interband term and making $E_F = 0$ is equivalent to removing the graphene sheets, therefore making disorder in random widths of air meaningless. Hence the localization length diverges, as can be seen in Eq. (24), where $\sigma \to 0$ implies in a vanishing Lyapunov exponent.

3. *One-layer system with compositional disorder*

In the compositional disorder regime and for the one-layered system, ξ decreases as β increases. For the TE mode, β can only be greater than 1 for materials with magnetic response, $\mu > 1$. For the TM mode, β is proportional to the dielectric constant and to $\cos\theta$, thus for grazing incidence the system becomes fully opaque.

In the Drude regime, the asymptotic behavior of the localization length goes as ω^2. This can be understood as follows: as the frequency increases, the graphene conductivity

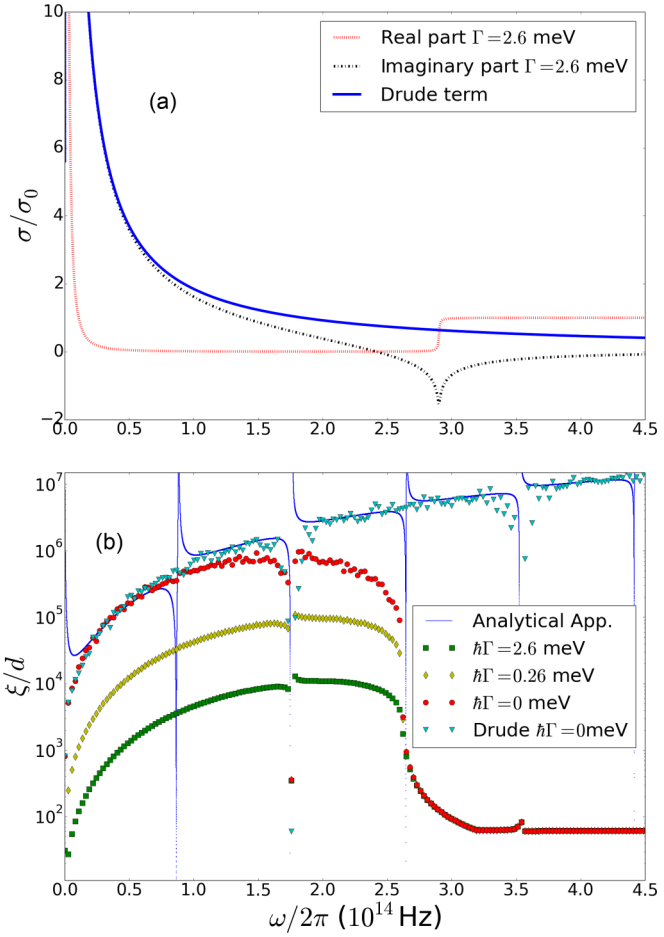

FIG. 6. (Color online) (a) Real and imaginary parts of the graphene optical conductivity in the compositional disordered case, $\sigma = \sigma_D + \sigma_I$, and the Drude conductivity σ_D when $\Gamma = 0$. (b) Localization length as a function of frequency with $z^0 = 1.2$ μm, $\theta = \pi/4$, $\varepsilon = \mu = 1$, $E_F^0 = 0.6$ eV, $\Upsilon_F = 0.12$ eV, and $N = 5000$ and increasing relaxation rate Γ. $\omega_F \approx 3 \times 10^{14}$ Hz. The blue triangles (and solid blue line) refer to a calculation in which only the Drude conductivity with $\Gamma = 0$ is used. The other data sets refer to the use of the full optical conductivity of graphene with different Γ values.

decreases as ω^{-1} and thus the influence of the graphene layer disappears.

The effect of compositional disorder is shown in Fig. 6, where the Fermi energy is randomly distributed around the mean value $E_F^0 = 0.6$ eV. ξ is inversely proportional to the mean standard deviation of the Fermi energy. We study the effect of increasing absorption in graphene layers, which depends on the real part of the conductivity and is proportional to the relaxation rate Γ. The length ξ decays rapidly when the frequency reaches $2\omega_F$, and interband transitions start to occur, an effect that may be related either to absorption or to Anderson localization. The numerical calculation is performed with the full graphene conductivity (Drude plus interband) and then compared to the case in which only the Drude term is present. The analytical approximation is calculated with the Drude term only, and it agrees very well with the numerical simulation except at the band edges $\gamma = 0, \pi/2, \pi$. As already discussed, this disagreement is related to the fact that the probability distribution of Θ_n is not uniform for these values of γ. The analytical approximation has a peak at $\gamma = \pi/2$ [see the denominator of Eq. (22)]. The numerical calculations show that near the band gap [$\gamma = 0, \pi$ see Eq. (22)] ξ goes to zero, and the peak at $\gamma = \pi/2$ does not occur.

D. Complex interband regime when Re $\sigma \approx 0$, Im $\sigma < 0$

When $\omega \lesssim 2\omega_F$, the imaginary part of the optical conductivity of graphene becomes negative and can be approximated by

$$\sigma = i\sigma_I'' + i\sigma_0 \frac{4}{\pi} \frac{\omega_F}{\omega}, \tag{34}$$

where σ_I'' is given by Eq. (D4). In this case, the imaginary part of σ becomes negative, and the ratio between the imaginary and real parts of σ becomes lower than in the Drude regime for typical values of Γ and E_F. Therefore, in this case the exponential decay of transmission is essentially due to absorption rather than to Anderson localization. Therefore, in this case, our approach for studying Anderson localization using the localization length is inadequate. It is worth commenting that experimentally it is possible to distinguish between absorption and Anderson localization by investigating the variance of the normalized total transmission, as proposed in Ref. [36]. For a one-layered system in the ATR regime with the transfer matrix given by Eq. (C9), the change in the sign of f has qualitatively the same effect in the dispersion relation (C10) of interchanging TE and TM modes, which changes the sign of β.

When the frequency becomes larger than $2\omega_F$, the real part of the conductivity approaches σ_0 while the imaginary part vanishes. In this regime, the role of the graphene sheets consists, essentially, in absorbing light leading to a vanishing transmission after a few stacks.

IV. CONCLUSIONS

In conclusion, we have investigated light propagation in 1D disordered superlattices composed of dielectric stacks and graphene sheets in between. We introduced disorder either in the graphene material parameters (compositional disorder), such as the Fermi energy, or in the widths of the dielectric stacks (structural disorder). For both cases, we derived an analytical expression for the localization length ξ and compared the results with numerical calculations based on the transfer-matrix method. A very good agreement between numerics and the analytical expression was found. We demonstrated that, for structural disorder and when the impedances of the layers are equal, the localization length does not follow the well-known asymptotic behavior $\xi \propto \omega^{-2}$. Rather, it exhibits an oscillatory dependence on frequency as a result of the presence of the Drude term in the graphene conductivity. Also in the impedance matching regime, we show that graphene has an important impact on the Brewster modes, anomalously delocalized modes at given frequencies, and incident angles at which ξ diverges. Indeed, the presence of graphene induces additional reflections inside the disordered medium, leading to a strong attenuation of the Brewster modes.

We investigated how intraband and interband transitions in the graphene conductivity impact ξ, identifying the regimes where Anderson localization and absorption dominates light transmission. Altogether, our findings unveil the role of graphene on Anderson localization of light, paving the way for the design of graphene-based, disordered photonic devices in the THz spectral range.

ACKNOWLEDGMENTS

We thank W. Kort-Kamp for useful discussions. A.J.C. acknowledges the scholarship from the Brazilian agency CNPq (Conselho Nacional de Desenvolvimento Científico e Tecnológico). N.M.R.P. acknowledges financial support from the Graphene Flagship Project (Contract No. CNECT-ICT-604391). F.A.P. thanks the Optoelectronics Research Centre and Centre for Photonic Metamaterials, University of Southampton, for the hospitality, and CAPES for funding his visit (Grant No. BEX 1497/14-6). F.A.P. also acknowledges CNPq (Grant No. 303286/2013-0) for financial support.

APPENDIX A: MATRIX TRANSFORMATION

The relation $\psi^{n+1} = M^n\psi^n$ can be interpreted as a discrete set of points in phase space, ψ_R, ψ_L. With the transformation $M_{\rm real}$,

$$M_{\rm real} = \frac{1}{2}\begin{pmatrix} 1-i & 1+i \\ -1+i & 1+i \end{pmatrix}, \tag{A1}$$

the matrix $M_{\rm real}M^nM_{\rm real}^{-1}$ is now real, and defining $\psi'^n = M_{\rm real}\psi^n$ we have in phase space ψ'_R, ψ'_L, where the trajectory is given by an ellipse in the system without disorder. From this we can find a transformation $M_{\rm circle}$ to a circle,

$$M_{\rm circle} = \begin{pmatrix} v^{-1}\cos\tau & v\sin\tau \\ -v^{-1}\sin\tau & v\cos\tau \end{pmatrix}, \tag{A2}$$

where

$$\begin{aligned} v^2 &= -\frac{\sin\gamma}{\cosh\phi_1^0\sin\phi_2^0 + \sinh\phi_1^0}, \\ \tau &= \frac{\pi}{4} - \frac{\phi_3^0}{2}, \end{aligned} \tag{A3}$$

and making $[Q \;\; P]^T = M_{\rm circle}\psi'$,

$$\begin{pmatrix} Q_n \\ P_n \end{pmatrix} = \begin{pmatrix} v^{-1}\cos\tau & v\sin\tau \\ -v^{-1}\sin\tau & v\cos\tau \end{pmatrix}\begin{pmatrix} x_n \\ y_n \end{pmatrix}. \tag{A4}$$

APPENDIX B: LYAPUNOV EXPONENT

The Lyapunov exponent is given by

$$\lambda = \tfrac{1}{2}\big\langle Y_1 + Y_2\cos 2\Theta_n + Y_3\sin 2\Theta_n - \tfrac{1}{4}Y_2^2 - \tfrac{1}{4}Y_3^2\big\rangle, \tag{B1}$$

where

$$Y_1 = \frac{1}{\sin^2\gamma}\big[U_1\delta\phi_1^2 + U_2\delta\phi_2^2 + U_3\delta\phi_3^2 + U_4\delta\phi_1\delta\phi_2\big], \tag{B2}$$

with

$$U_1 = 2\sin^2\phi_2^0, \tag{B3}$$

$$U_2 = 2\sinh^2\phi_1^0\cos^2\gamma, \tag{B4}$$

$$U_3 = 2\sinh^2\phi_1^0\sin^2\gamma, \tag{B5}$$

$$U_4 = -\sinh 2\phi_1^0\sin 2\phi_2^0, \tag{B6}$$

$$Y_2 = \big[-2\sin\phi_2^0\delta\phi_1 + \cos\phi_2^0\sinh 2\phi_1^0(\delta\phi_2 - \delta\phi_3)\big], \tag{B7}$$

$$Y_3 = 2\frac{\sinh\phi_1^0(\cos^2\gamma\,\delta\phi_2 + \sin^2\gamma\,\delta\phi_3) - \cos\gamma\sin\phi_2^0\delta\phi_1}{-\sin\gamma}. \tag{B8}$$

The angle Θ obeys the recurrence equation

$$\Theta_{n+1} = \Theta_n - \gamma + \epsilon_n\csc\gamma, \tag{B9}$$

with

$$\begin{aligned} \epsilon_n = {} & \big[\cos\gamma\sinh\phi_1^0\delta\phi_2 - \sin\phi_2^0\delta\phi_1\big]\cos(2\Theta_n - \gamma) \\ & + \sinh\phi_1^0\cos\gamma\sin(2\Theta_n - \gamma)\delta\phi_3, \end{aligned} \tag{B10}$$

APPENDIX C: PHOTONIC CRYSTAL

1. Unit cell made of two different dielectrics and a graphene sheet at the interfaces

In this appendix, we present the transfer matrix whose elements are [3][1]

$$\begin{aligned} m_{11}^j &= [A_-^x\cos\alpha_2 + i(\chi + C_+^x)\sin\alpha_2]e^{-i\alpha_1}, \\ m_{12}^j &= [B^x\cos\alpha_2 + i(\Delta + D^x)\sin\alpha_2]e^{i\alpha_1}, \\ m_{21}^j &= [-B^x\cos\alpha_2 - i(\Delta + D^x)\sin\alpha_2]e^{-i\alpha_1}, \\ m_{22}^j &= [A_+^x\cos\alpha_2 - i(\chi + C_-^x)\sin\alpha_2]e^{i\alpha_1}, \end{aligned} \tag{C1}$$

where $x = $ TE,TM, and the diverse parameters.

The Snell-Decartes law holds,

$$\sqrt{\varepsilon_1\mu_1}\sin\theta_1 = \sqrt{\varepsilon_2\mu_2}\sin\theta_2, \tag{C2}$$

and the dispersion relation is given by

$$\begin{aligned} \cos\gamma = {} & \cos\alpha_1\cos\alpha_2 - \big(\chi + 2f^2\beta_1^x\beta_2^x\big)\sin\alpha_1\sin\alpha_2 \\ & + 2if\big(\beta_1^x\cos\alpha_1\sin\alpha_2 + \beta_2^x\cos\alpha_2\sin\alpha_1\big). \end{aligned} \tag{C3}$$

$$\beta_i^{\rm TM} = Z_i^{\rm TM}, \;\; \beta_i^{\rm TE} = \frac{1}{Z_i^{\rm TE}}, \tag{C4}$$

[1]There are some typos in the transfer-matrix elements given in Ref. [3].

where

$$
\begin{aligned}
k_i &= \sqrt{\varepsilon_i \mu_i}\omega/c\cos\theta_i,\\
\alpha_i &= k_i z_i,\\
A^x_{\pm} &= \left(1 \pm 2f\beta^x_1\right),\\
B^x &= 2f\lambda^x\beta^x_1,\\
C^x_{\pm} &= \pm 2f\beta^x_2 + 2f^2\beta^x_1\beta^x_2,\\
D^x &= 2f^2\lambda^x\beta^x_1\beta^x_2,\\
\eta^x &= \frac{Z^x_1}{Z^x_2},\\
\Delta^x &= \frac{1}{2}(\eta^x - \eta^{x-1}),\\
\chi^x &= \frac{1}{2}(\eta^x + \eta^{x-1}),\\
f &= \frac{\sigma c\mu_0}{2},\\
Z^{\mathrm{TE}}_i &= \frac{\sqrt{\mu_i\varepsilon_i}}{\mu_i}\cos\theta_i,\\
Z^{\mathrm{TM}}_i &= \frac{\sqrt{\mu_i\varepsilon_i}}{\varepsilon_i}\cos\theta_i,
\end{aligned}
\tag{C5}
$$

with $\lambda^{\mathrm{TM}} = +1, \lambda^{\mathrm{TE}} = -1$.

The graphene transfer matrix between two media $(1 \to 2)$ is given by

$$
M = \frac{1}{2}\begin{pmatrix} 1+\eta^x - 2\beta^x_2 f & \eta^x - 1 - 2\beta^x_2 f \\ \eta^x - 1 + 2\beta^x_2 f & 1 + \eta^x + 2\beta^x_2 f \end{pmatrix}. \tag{C6}
$$

The Fresnel transmission (t) and reflection (r) amplitudes read

$$
t = \frac{1}{1+\eta^x + 2\beta^x_2 f}, \tag{C7}
$$

$$
r = \frac{1-\eta^x - 2\beta^x_2 f}{1+\eta^x + 2\beta^x_2 f}. \tag{C8}
$$

2. Unit cell made of one dielectric and a graphene sheet at the interface

When there is only one dielectric, with width z and ε,μ permissivity and permeability, intercalated by graphene sheets, the transfer matrix is given by

$$
M = \begin{pmatrix} (1-\beta^x f)e^{i\alpha} & -\lambda^x\beta^x f e^{i\alpha} \\ \lambda^x\beta^x f e^{-i\alpha} & (1+\beta^x f)e^{-i\alpha} \end{pmatrix}, \tag{C9}
$$

where $\alpha = \sqrt{\mu\varepsilon}z\cos\theta$, and β^x is defined in (C4) where we dropped the i index because we deal with only one layer. The dispersion relation is

$$
\cos\gamma = \cos\alpha - i\beta^x f\sin\alpha. \tag{C10}
$$

APPENDIX D: GRAPHENE OPTICAL CONDUCTIVITY

For completeness, in this appendix we give the expressions for the optical conductivity of graphene, whose derivation can be found elsewhere [37,38]. The graphene optical conductivity of graphene is a sum of a Drude term, σ_D, and an interband contribution, σ_I, reading

$$
\sigma = \sigma_D + \sigma_I, \tag{D1}
$$

where the Drude term is given by

$$
\frac{\sigma_D}{\sigma_0} = \frac{4\omega_F}{\pi}\frac{1}{\Gamma - i\omega}, \tag{D2}
$$

and the interband term $\sigma_I = \sigma'_I + i\sigma''_I$ has the real part

$$
\frac{\sigma'_I}{\sigma_0} = \left(1 + \frac{1}{\pi}\arctan\frac{\omega - 2\omega_F}{\Gamma} - \frac{1}{\pi}\arctan\frac{\omega + 2\omega_F}{\Gamma}\right) \tag{D3}
$$

and the imaginary part

$$
\frac{\sigma''_I}{\sigma_0} = -\frac{1}{2\pi}\ln\frac{(2\omega_F+\omega)^2 + \Gamma^2}{(2\omega_F - \omega)^2 + \Gamma^2}, \tag{D4}
$$

with the Fermi frequency given by

$$
\omega_F = \frac{|E_F|}{\hbar}. \tag{D5}
$$

[1] P. Avouris and M. Freitag, IEEE J. Sel. Top. Quantum Electron. **20**, 72 (2014).
[2] Y. V. Bludov, N. M. R. Peres, and M. I. Vasilevskiy, J. Opt. **15**, 114004 (2013).
[3] T. Zhan, X. Shi, Y. Dai, X. Liu, and J. Zi, J. Phys. Condens. Matter **25**, 215301 (2013).
[4] F. Xia, T. Mueller, Y. Lin, A. Valdes-Garcia, and P. Avouris, Nat. Nanotechnol. **4**, 839 (2009).
[5] M. Liu, X. Yin, E. Avila, B. Geng, T. Zentgraf, L. Ju, F. Wang, and X. Zhang, Nature (London) **474**, 64 (2011).
[6] F. Garcia de Abajo, ACS Photon. **1**, 135 (2014).
[7] L. Ju, B. Geng, J. Horng, C. Girit, M. Martin, Z. Hao, H. Bechtel, X. Liang, A. Zettl, Y. Shen, and F. Wang, Nat. Nanotechnol. **6**, 630 (2011).
[8] T. Echtermeyer, L. Britnell, P. Jasnos, A. Lombardo, R. Gorbachev, A. Grigorenko, A. Geim, A. Ferrari, and K. Novoselov, Nat. Commun. **2**, 458 (2011).
[9] Z. Sun, T. Hasan, F. Torrisi, D. Popa, G. Privitera, F. Wang, F. Bonaccorso, D. Basko, and A. Ferrari, ACS Nano **4**, 803 (2010).
[10] M. Engel, M. Steiner, A. Lombardo, A. Ferrari, H. Lohneysen, P. Avouris, and R. Krupke, Nat. Commun. **3**, 906 (2012).
[11] A. Majumdar, J. Kim, J. Vuckovic, and F. Wang, Nano Lett. **92**, 68001 (2013).
[12] X. Gan, R. Shiue, Y. Gao, K. Mak, X. Yao, L. Li, A. Szep, D. Walker, J. Hone, T. Heinz, and D. Englund, Nano Lett. **13**, 69 (2013).
[13] P. Anderson, Phys. Rev. **109**, 1492 (1958).
[14] S. John, Phys. Rev. Lett. **53**, 2169 (1984).

[15] M. Segev, Y. Silberberg, and D. Christodoulides, Nat. Photon. **7**, 197 (2013).
[16] H. Deng, X. Chen, B. A. Malomed, N. C. Panoiu, and F. Ye, Sci. Rep. **5**, 15585 (2015).
[17] H. Hu, A. Strybulevych, J. Page, S. Skipetrov, and B. van Tiggelen, Nat. Phys. **4**, 945 (2008).
[18] J. Billy, V. Josse, Z. Zuo, A. Bernard, B. Hambrecht, P. Lugan, D. Clement, L. Sanchez-Palencia, P. Bouyer, and A. Aspect, Nature (London) **453**, 891 (2008).
[19] A. Lagendijk, B. van Tiggelen, and D. Wiersma, Phys. Today **62**, 24 (2009).
[20] F. Izrailev, A. Krokhin, and N. Makarov, Phys. Rep. **512**, 125 (2012).
[21] J. Bertolotti, S. Gottardo, D. S. Wiersma, M. Ghulinyan, and L. Pavesi, Phys. Rev. Lett. **94**, 113903 (2005).
[22] A. A. Asatryan, L. C. Botten, M. A. Byrne, V. D. Freilikher, S. A. Gredeskul, I. V. Shadrivov, R. C. McPhedran, and Y. S. Kivshar, Phys. Rev. Lett. **99**, 193902 (2007).
[23] A. A. Asatryan, L. C. Botten, M. A. Byrne, V. D. Freilikher, S. A. Gredeskul, I. V. Shadrivov, R. C. McPhedran, and Y. S. Kivshar, Phys. Rev. B **82**, 205124 (2010).
[24] D. Mogilevtsev, F. A. Pinheiro, R. R. dos Santos, S. B. Cavalcanti, and L. E. Oliveira, Phys. Rev. B **82**, 081105 (2010).
[25] D. Mogilevtsev, F. A. Pinheiro, R. R. dos Santos, S. B. Cavalcanti, and L. E. Oliveira, Phys. Rev. B **84**, 094204 (2011).
[26] A. A. Asatryan, L. C. Botten, M. A. Byrne, V. D. Freilikher, S. A. Gredeskul, I. V. Shadrivov, R. C. McPhedran, and Y. S. Kivshar, Phys. Rev. B **85**, 045122 (2012).
[27] A. A. Asatryan, N. A. Nicorovici, L. C. Botten, C. M. de Sterke, P. A. Robinson, and R. C. McPhedran, Phys. Rev. B **57**, 13535 (1998).
[28] V. Kuzmiak and A. A. Maradudin, Phys. Rev. B **55**, 7427 (1997).
[29] D. Soto-Puebla, F. Ramos-Mendieta, and M. Xiao, Int. J. Mod. Phys. B **18**, 125 (2004).
[30] P. Markos and C. M. Soukoulis, *Wave Propagation: From Electrons to Photonic Crystals and Left-handed Materials* (Princeton University Press, Princeton, NJ, 2008).
[31] F. M. Izrailev and N. M. Makarov, Phys. Rev. Lett. **102**, 203901 (2009).
[32] F. M. Izrailev, T. Kottos, and G. P. Tsironis, Phys. Rev. B **52**, 3274 (1995).
[33] F. M. Izrailev, S. Ruffo, and L. Tessieri, J. Phys. A **31**, 5263 (1998).
[34] J. E. Sipe, P. Sheng, B. S. White, and M. H. Cohen, Phys. Rev. Lett. **60**, 108 (1988).
[35] Y. V. Bludov, M. Vasilevskiy, and N. Peres, Europhys. Lett. **92**, 68001 (2010).
[36] A. A. Chabanov, M. Stoytchev, and A. Z. Genack, Nature (London) **404**, 850 (2000).
[37] N. M. R. Peres, Rev. Mod. Phys. **82**, 2673 (2010).
[38] Y. V. Bludov, A. Ferreira, N. M. R. Peres, and M. I. Vasilevskiy, Int. J. Mod. Phys. B **27**, 1341001 (2013).